Ionic Liquid Electrolyte for Room to Intermediate Temperature Operating Li Metal Batteries: Dendrite Suppression and Improved Performance

Jinkwang Hwang, Haruki Okada, Ryutaro Haraguchi, Shinya Tawa, Kazuhiko Matsumoto,* Rika Hagiwara

Graduate School of Energy Science, Kyoto University, Yoshida-honmachi, Sakyo-ku, Kyoto 606-8501, Japan.

*Corresponding authors: Kazuhiko Matsumoto

E-mail: k-matsumoto@energy.kyoto-u.ac.jp

Tel: +81757534817

Fax: +81757535906

Abstract

Lithium metal is considered to be the ultimate negative electrode material to maximize the energy density of lithium secondary batteries based on its high theoretical specific capacity and low redox potential. Despite these outstanding features, lithium metal is facing difficulties in overcoming of dendritic lithium growth, low coulombic efficiency, and poor cycle performance. In this study, the Li[FSA]-[1-ethyl-3-methylimidazolium][FSA] (FSA^- = bis(fluorosulfonyl)amide) ionic liquid system is proposed to be an electrolyte for wide temperature operable Li metal batteries. The ionic liquid presents unique properties of suppressing Li dendrite growth, dead Li accumulation, and long-life cycling performance across 25 and 90 °C. Full-cell tests with $Li_2FeP_2O_7$ positive electrode and this ionic liquid electrolyte demonstrate the feasibility of operating lithium metal batteries from room to intermediate temperature. The full cell retained 99.8% of its initial capacity after 200 cycles with an average coulombic efficiency of 99.7%.

Keywords:

Lithium metal anode; Secondary batteries; Ionic liquids; Dendrite suppression; Li deposition/dissolution

1. Introduction

There have been many attempts to use Li metal as a negative electrode in batteries based on its tenfold higher charged-state capacity than graphite (3860 vs. 340 mAh g^{-1}) [1-4]. However, Li metal has practical drawbacks because Li metal electrodes function on the basis of metal deposition/dissolution rather than ion-intercalation. Li dendrites formed in this process are converted into a dead Li layer, which limits performance by the continuous consumption of electrolyte, which leads to low Coulombic efficiency (CE), and a volumetric change causes severe safety risks due to short-circuiting [4-6]. Consequently, a graphite negative electrode is occupying the majority of the market of Li-ion batteries [3, 7]. However, the use of Li metal can meet the high energy density demands of industry and society and contributes significant advantages to conventional Li-based batteries, including Li-air and Li-sulfur batteries [8-10].

Extensive studies of Li metal electrodes have been conducted to overcome the problem of dendrite formation and to increase cycling performance. Electrolytes play a crucial role in the negative electrode function by forming a stable solid electrolyte interphase (SEI) layer. Li salts including $LiClO_4$, $LiPF_6$, $LiAsF_6$, and Li[FSA] dissolved in organic solvents such as ethylene carbonate (EC), dimethyl carbonate (DMC), diethyl carbonate (DEC), 1,2-dimethoxyethane (DME), and vinyl carbonate (VC) (sometimes with additives present) have been tested to find the best conditions for creating a stable SEI layer on Li electrode surfaces [11-17]. Artificial SEI layer formation and Li surface modification also have been pursued as a means of inhibiting dendrite growth and suppressing volumetric changes [18-20]. Lately, some works of literature have reported that ether-based electrolytes and ionic liquid electrolytes can form a robust passivation layer on the lithium metal electrode, enabling stable Li dissolution/deposition cycles (Table S1, a brief summary of Li deposition/dissolution tests

using ether-based electrolytes and ionic liquids electrolytes) [17, 21-27]. However, the organic electrolytes currently used in Li-ion batteries are not an optimum choice when used in conjunction with Li metal electrodes because highly volatile and flammable organic electrolytes are not desirable from the standpoint of safety at intermediate temperature operation [28-30]. Ionic liquid electrolytes is an interesting candidate for this purpose as ionic liquids form an electrochemically stable SEI layer and suppress Li dendrite formation [28, 31-35]. Recently, Basile et al. reported that lithium metal immersed in the $[C_3C_1Pyrr][FSA]$ ($C_3C_1Pyrr^+$ = *N*-propyl-*N*-methylpyrrolidinium) ionic liquid for 12 days exhibits stable symmetric Li/Li cell cycling and greatly suppresses lithium dendrite formation [31].

This study reports on the suppression and mechanism of Li metal dendrite formation utilizing a nonflammable and electrochemically and thermally stable ionic liquid electrolyte of 30 mol% Li[FSA]-$[C_2C_1im][FSA]$ (hereafter abbreviated as IL) [31]. A conventional organic carbonate electrolyte of 1 mol dm^{-3} $Li[PF_6]$-EC/DMC (1:1 vol/vol) (hereafter abbreviated as OE), was selected for comparison and addresses the safety and efficiency aspects of Li metal battery operation from 25 to 90 °C. Because Li metal battery operation at intermediate temperatures is more challenging than that of Li-ion batteries as safety concerns and could mean that safe operation at room temperature is guaranteed. Furthermore, a high rate capability can be achieved via enhanced electrode reaction and ion diffusion at elevated temperatures where can be a ubiquitous presence of waste heat in our daily lives and industries.

The enhanced Li metal deposition/dissolution properties in IL motivated us to conduct full-cell tests with Li metal as the negative electrode and untreated $Li_2FeP_2O_7$ (LFP, theoretical capacity = 110 mAh g^{-1}) as the positive electrode [36]. When prepared without sophisticated treatments such as nanonization and carbon coating, the limited room temperature capacity of

LFP readily declines in OE and IL even at low current. This makes the LFP is suitable for investigating the effects of temperature and the charge/discharge behavior of a Li metal electrode on types of electrolytes.

2. Results and discussion

Symmetric Li/Li cells were prepared in a glass beaker cell (Fig. S1) to observe the formation of Li dendrites and the accumulation of dead Li as electrodes degraded and electrolyte consumed during the cycling test. Li metal was deposited and dissolved at two Li metal electrodes at 8.0 mA cm^{-2} for 210 min (8 min per cycle) (Fig. 1a). Photos selected from a video recording of the cycling test show that the OE and IL cells exhibit completely different Li deposition/dissolution behaviors throughout the test (Fig. 1a). (Supplementary data provides a full video).

The OE cell shows uneven Li metal deposition at an early stage and the continual growth of Li dendrites and accumulation of dead Li, which hindered Li^+ diffusion and ultimately caused a short circuit (Fig. 1). The overpotential of the OE cell continuously increases during cycling, owing to dead Li accumulation (Fig. S2a). The IL cell exhibits very stable cycling behavior and uniform Li metal deposition. Although Li nucleation is confirmed in the early stage, the increase of the amount of the deposited Li metal on the electrode in the IL cell is not visible, and the dendrite formation is suppressed at a minimum level without dead Li layer (Fig. 1). This result accords with the invariant overpotential (Fig. S2b) and indicates the IL could suppress the formation of Li dendrites with uniform Li deposition and stable SEI formation [37].

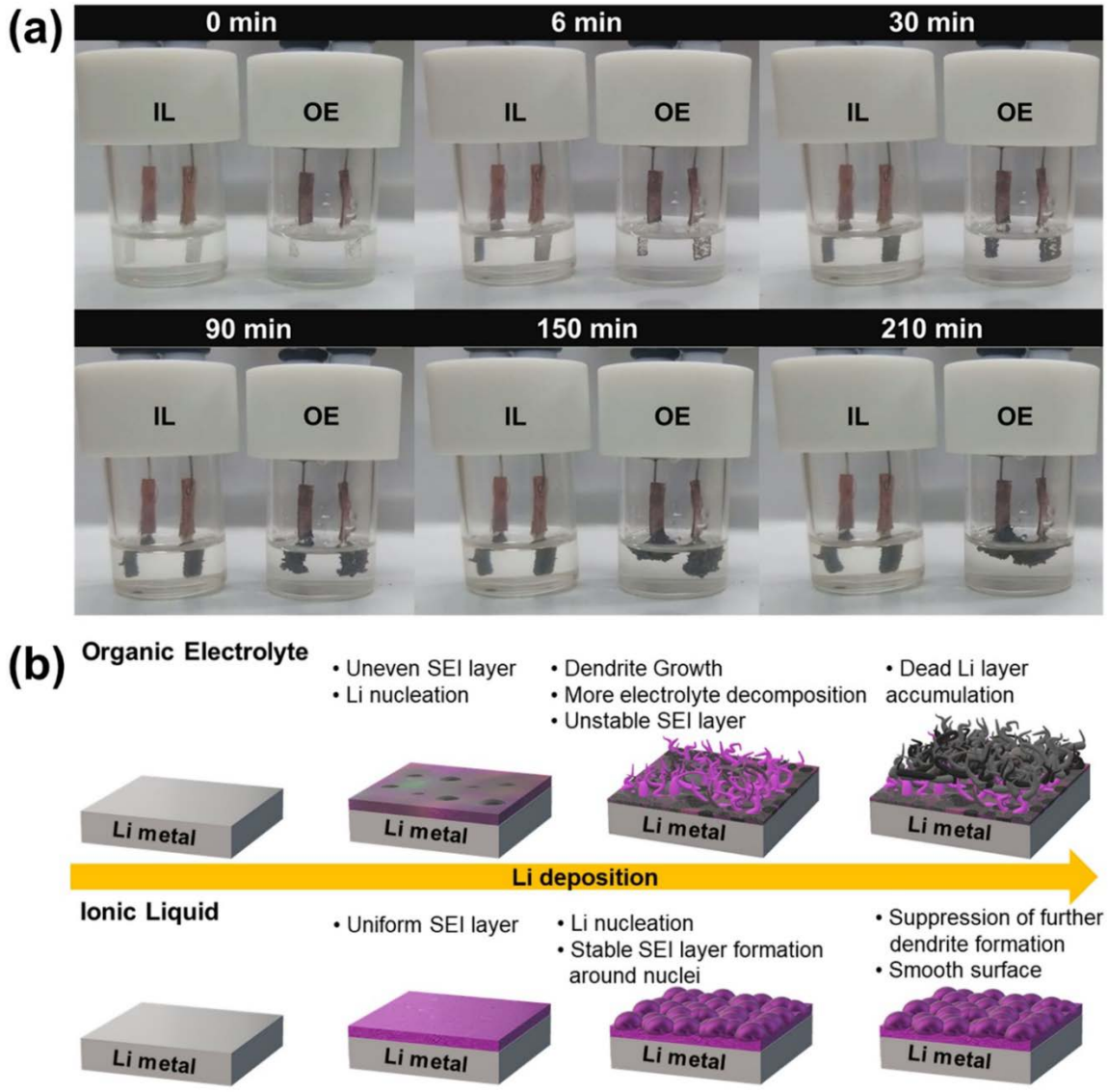

Fig. 1. (a) Dendrite formation in symmetric Li/Li cells during cycling at 8.0 mA cm^{-2} at 25 °C. (b) Schematic comparison of Li deposition and dendrite formation with OE and IL. See Fig. S2 for the corresponding voltage profiles.

Further evaluation was performed by long-term deposition/dissolution test using symmetric Li/Li cells in coin-cell configuration at current densities of 1.0 and 5.0 mA cm^{-2} for OE at 25 °C and IL at 25 and 90 °C in Fig. S3. The OE cell response is stable for only a limited number of cycles. The overpotential began to increase after 25 h and reached 0.2 V after 246 h

at 1.0 mA cm^{-2} and increases after only 18 min and reaches 0.3 V after 50 h at 5.0 mA cm^{-2} (Fig. S3a,d). The increases in overpotential indicate severe decomposition of the electrolyte, the continual formation of Li dendrites, and dead Li accumulation in the OE cell [38]. On the other hand, the IL cells at 25 and 90 °C exhibit stable cycling performance (Fig. S3b,c,e,f). The large overpotential during the early cycles in the IL cell at 25°C should originate from SEI formation, poor contact between the electrode and electrolyte, or kinetic limitations in the cell as previously reported [39, 40]. The profiles of the IL cell are stabilized after the 50th cycle at 25 °C and exhibit a constant overpotential of 12 mV that did not increase for 1000 h (2500 cycles) at 1.0 mA cm^{-2} (Fig. S3b). The overpotential becomes smaller (3 mV) at 90 °C at 1.0 mA cm^{-2} (Fig. S3c), which is consistent with enhanced ion diffusion in the electrolyte and more effective charge transfer at the IL/Li interface with increasing temperature. IL cells exhibited stable performance at a higher current density of 5.0 mA cm^{-2}. The overpotential of 42 mV is maintained until 1400 h and starts to gradually increase and reaches 84 mV after 2200 h at 25 °C in Fig. S3e. The overpotential of 16 mV is reserved until 2000 h at 90 °C in Fig. S3f.

The cycle efficiency (ε_{cycle}) during Li deposition/dissolution is shown in Fig. S4 (See for the method of evaluating ε_{cycle}). The value of ε_{cycle} is obtained to 71% in OE at 25 °C. The value increases to 92% in IL at 25 °C because IL could facilitate smooth Li deposition/dissolution, as shown in Fig. 1, but elevating temperature triggers the consumption of Li during the cycle and shows ε_{cycle} value of 72%.

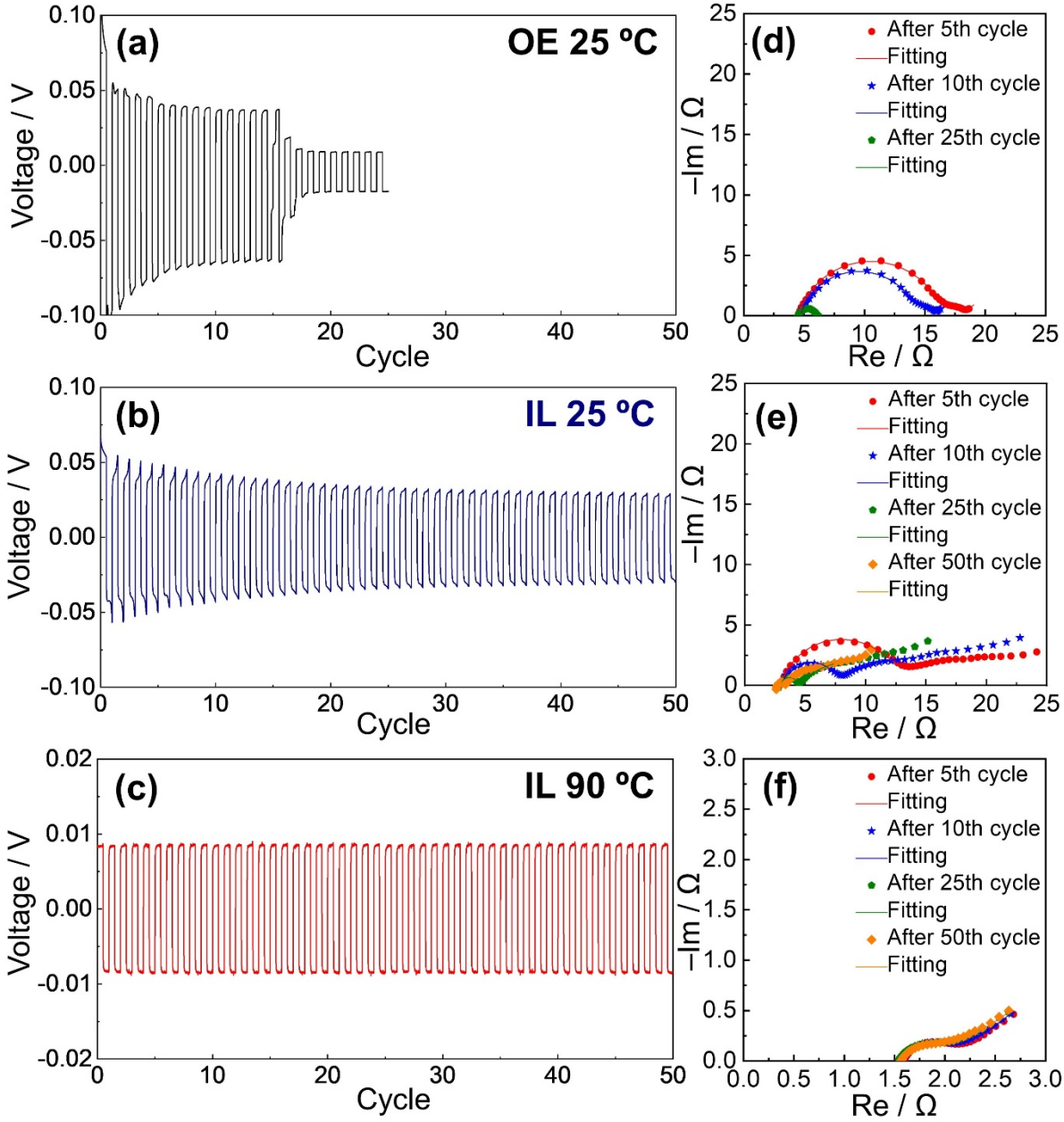

Fig. 2 Voltage profiles of symmetric Li/Li cells cycled at 1.0 mA cm^{-2} (24 min per cycle) for (a) OE at 25 °C, (b) IL at 25 °C, and (c) IL at 90 °C. Nyquist plots upon cycles (d) OE at 25 °C, (e) IL at 25 °C, and (f) IL at 90 °C. See Fig. S3 for the long-term cycling tests for a Li/Li cell in coin-cell configuration and Table S2 for the EIS parameters.

Electrical impedance spectroscopy (EIS) upon cycle tests are shown in Fig. 2. The Nyquist plots of the Li/Li symmetric cells exhibit two semicircles. (See Table S2 for the EIS parameters). The two semicircles are distinct at 25 °C, whereas they partially overlap each

other without a definite border at 90 °C. A semicircle with the characteristic frequency range of 200 to 10 kHz corresponds to the high-frequency resistance (R_h) that is characteristic of the chemical or electrochemical formation of a passivation film. Semicircles at 200 to 1 Hz are characteristic of the charge transfer resistance (R_{ct}) [41, 42]. The EIS results and voltage profiles indicate that passivation films are formed on Li metal electrodes just after the electrode contact with the electrolytes during cell assembly, which reflects in the large R_h value and the large overpotential at initial cycles at 25 °C in OE and IL (Fig. 2d,e, and S3a,b,d,e). R_h decreases during the initial cycles, as observed in other ionic liquids [31]. This suggests that the pristine passivation layer presents a barrier to diffusion that is reduced by Li deposition/dissolution during the initial cycles to form a new SEI layer, which is more amenable to Li^+ diffusion [43]. However, a dramatic decrease of the Nyquist plot is observed in the OE cell after 25^{th}, corresponding to the decrease in overpotential in the voltage profile after the 16th cycle. This indicates a short-circuit in the OE cell (Fig. 2a,d). In IL cell at 25 °C, R_h decreases rapidly as the cycle proceeds while the interfacial process is slightly improved by a decrease in R_{ct} from 7.65 to 6.99 Ω. (Fig. 2e). The consecutive overpotential decrease in the voltage profile in IL at 25 °C could be related to decrease in R_h (Fig. 2b,e). Elevating operating temperature to 90 °C decreases R_h and R_{ct} and the overpotential preserves until the end of test (Fig. 2c,f).

The scanning electron microscope (SEM) images show apparent differences in Li morphology resulting from different Li deposition/dissolution properties of the OE and IL and of the operating temperature. The Li metal surface after cycled in OE is rough and unevenly covered by Li deposits (Figs. 3a and S5a). These images show glass fiber in the deposited layer and a rough surface, which indicates severe Li dendrite growth and dead Li accumulation in the OE cell. However, the surface of the Li electrode cycled in IL was less rough in both the

SEM and optical images at 25 °C (Figs. 3b and S5b). The deposited and substrate layers are clearly distinguishable (Fig. 3b), as confirmed by energy-dispersive X-ray spectrometry (EDS). The elemental components of the SEI layer (C, N, F, and S) are detected in the deposited Li layer, but not in the Li substrate. These results suggest the IL suppresses Li dendrite formation and facilitates Li dissolution/deposition at the electrode in Fig. S6. The SEM images in Figs. 3c and S5c indicate that more Li dendrite is formed in IL cell at 90 °C than at 25 °C.

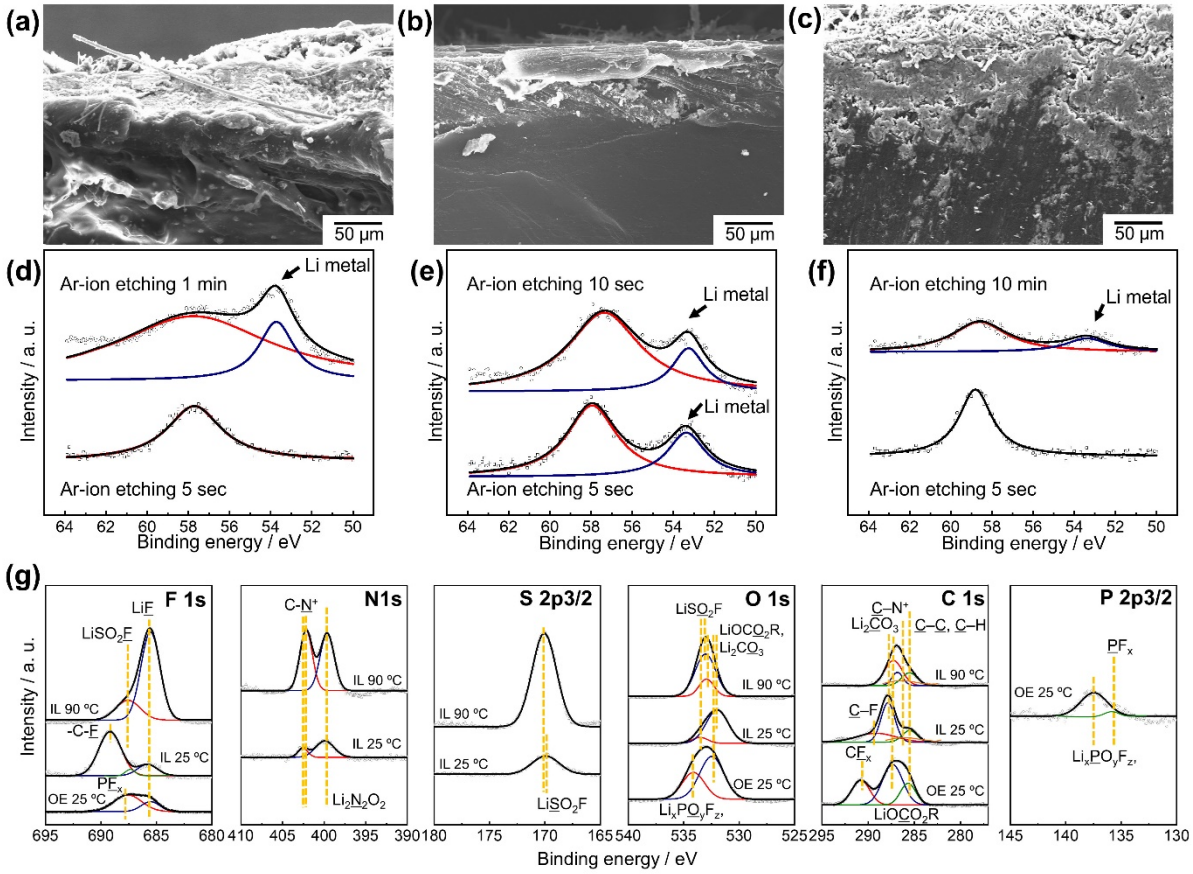

Fig. 3. The cross-sectional SEM images of the Li metal electrodes after cycles (a) OE at 25 °C, (b) IL at 25 °C, and (c) IL at 90 °C. Li 1s XPS spectra of Li metal electrodes subjected to Ar-ion etching for (d) OE at 25 °C, (e) IL at 25 °C, and (f) IL at 90 °C. Fitting lines in (d)-(f) correspond to total (black), Li metal (blue), and LiF (red) signals. (g) XPS spectra of the Li metal electrodes after cycle test; F 1s, N 1s, S $2p_{3/2}$, O 1s, C 1s, and P $2p_{3/2}$.

X-ray photoelectron spectroscopy (XPS) was used to determine the depth profile of the SEI layer. An argon-ion beam was applied to the electrode until Li 1s peaks appeared at ~53 eV [44, 45]. The electrode cycled in OE shows a Li metal peak after 1-min Ar-ion etching (Fig. 3d), whereas the electrode cycled in IL at 25 °C shows a Li metal peak after only 5 s (Fig. 3e). These results indicate that the OE decompose more extensively than IL in forming SEI layer and that the IL formed a stable, yet thin, SEI layer, which is favorable for Li^+ diffusion and contributes partially to the lower overpotential of the IL system in the symmetric cell test at 25 °C. The Li metal XPS peak appears after 10-min Ar-ion etching in IL at 90 °C (Fig. 3f) because the elevated operating temperature enhances the chemical reaction between Li metal and the IL, which consumed more electrolyte and Li metal in forming a stable SEI layer. However, the thick SEI layer could not hinder Li^+ diffusion at 90 °C, because of the increase in Li^+ diffusivity with temperature.

Chemical species at the Li metal surface were further analyzed by XPS spectroscopy (Fig. 3g) and EDS (Fig. S7). The formation of LiF by decomposition of the OE and IL electrolytes was confirmed by the Li 1s and F 1s XPS signals and by EDS (Fig. 3g and S7) in agreement with previous works [31, 37, 45-47]. The major difference in the composition of the SEI layers in the IL and OE cells is the presence of N- and S-containing species in the IL cells, as the OE contains no nitrogen or sulfur. The N 1s and S $2p_{3/2}$ spectra indicate that the SEI layer of the IL cells contains $LiSO_2F$, $C–N^+$ (im), and $Li_2N_2O_2$, which arise from the decomposition of the FSA^- anion and $C_2C_1im^+$ cation and contribute to the stable electrochemical performance of the IL cell. The elemental composition of the SEI layer formed in IL electrolyte seems to be effectively independent of the operating temperature, although the layer was thicker at 90 °C. The additional details on SEI formation components are arranged in Table S3.

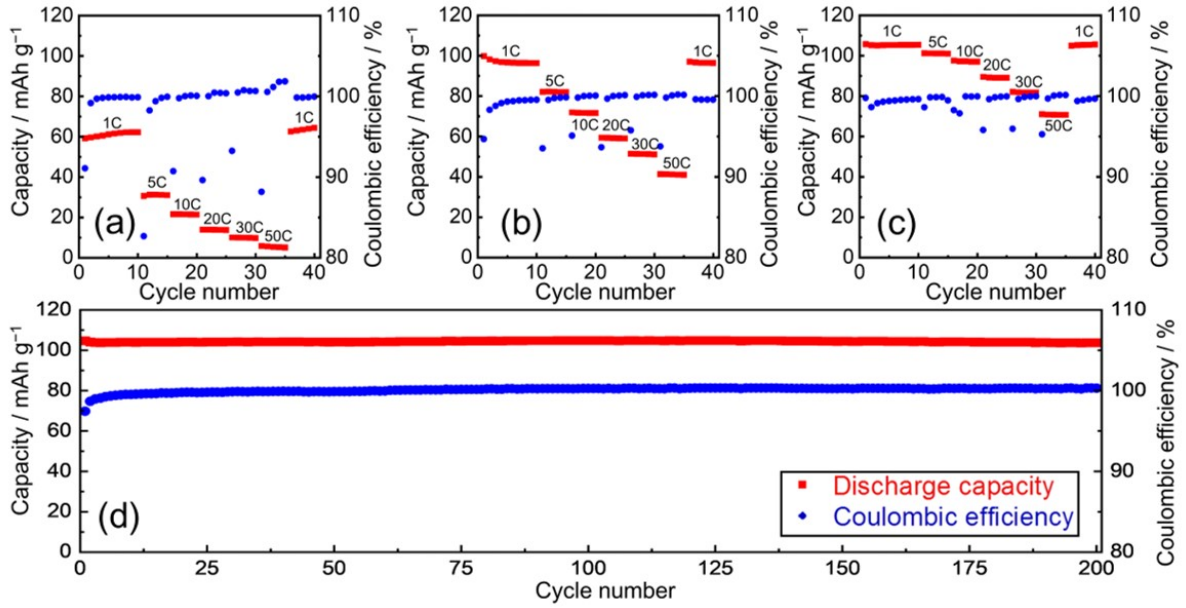

Fig. 4. Rate capability of the Li/IL/LFP cell at (a) 25, (b) 60, and (c) 90 °C. (d) Cyclability of the Li/IL/LFP cell at 1C at 90 °C. Cut-off voltage: 2.2–4.3 V. See Fig. S13 and S14 for charge/discharge curves.

Fig. 4 shows the results of full-cell tests with Li metal and LFP electrodes in a Li/IL/LFP cell at 25, 60, and 90 °C. Fig. S8−S11 illustrates the characterization of LFP. Fig. S12 displays the charge/discharge curves of a Li/OE/LFP cell at 25 °C. The Li/LFP combination delivers equivalent capacities with OE (57 mAh g^{-1}) and IL (61 mAh g^{-1}) at 25 °C. The capacity is improved to 97 mAh g^{-1} at 60 °C and 105 mAh g^{-1} at 90 °C in the IL cells at 1C. The temperature dependence of the charge/discharge curves decrease in slope with increasing temperature (~0.5, ~0.3, and ~0.2 V at 25, 60, and 90 C°, respectively, based on the voltages at 50% state of charge (SOC)), which suggests that polarization is suppressed at elevated temperature (Fig. S13). The rate capability of the Li/IL/LFP cells (Fig. 4a–c) is significantly improved at elevated operating temperatures. The capacity retention of 82% at 30C is realized at 90 °C with respect to that at 1C. Corresponding values of 10 and 51% are observed at 25 and 60 °C, respectively. The rapid recovery after the rate capability test attested

to the high thermal and chemical stability of this cell up to 90 °C. Temperature-dependent Nyquist plots of a symmetric LFP/IL/LFP cell (50% SOC) at 25, 50, 70, and 90 °C show the decrease in R_h and R_{ct} with increasing temperature (see the Nyquist plots in Fig. S15a,b and Bode plots in Fig. S15c,d, which suggests reduced polarization of the LFP electrode (Fig. S13). R_{ct} is substantially reduced at 90 °C, consistent with the superior rate performance of the Li/IL/LFP cell (Fig. 4c). Cycling performance at 90 °C was tested at 1C (Fig. 4d). Little capacity decay is observed for 200 cycles, and the CE reaches 99.0% at the 4th cycle and shows high average CE of 99.9% for 200 cycles. The capacity gradually fades during cycling becoming equal to 96% retention rate at the 200^{th} cycle based on theoretical capacity. However, cyclic testing with another ionic liquid of 30 mol% Li[FSA]-[C_3C_1pyrr][FSA] at 90 °C shows very limited cycling capability (Fig. S16).

Additionally, cycle tests of the traditional positive electrode of $LiFePO_4$ were carried out using the OE, IL, and 30 mol% Li[FSA]-[C_3C_1pyrr][FSA] electrolytes at 25, 60, and 90 °C (Fig. S17, Supplementary data). As reported with the LFP electrode, the $LiFePO_4$ electrode and IL (30 mol% Li[FSA]-[C_2C_1im][FSA]) electrolytes show high capacity retention and average coulombic efficiency at all the temperatures.

3. Conclusion

Li[FSA]-[C_2C_1im][FSA] IL was employed to construct a safe and room to intermediate temperature range operable Li-metal battery. The combination of Li metal and the IL presented excellent electrochemical behaviors. The IL exhibited lower polarization than corresponding cells containing OE at room temperature and showed a long life. These results accord with

effective suppression of Li dendrite growth and dead Li accumulation by the IL. Full-cell tests with untreated LFP as the positive electrode revealed clear differences in electrochemical behavior using different electrolytes and operating temperatures. The cell with IL exhibited better stability and charge/discharge capacity than a cell with an organic electrolyte even at room temperature at 25 °C. Moreover, cycling tests at 90 °C showed an excellent rate performance and high capacity retention. These results illustrate the benefits of using IL with Li metal electrode for safe Li-metal batteries.

Acknowledgements

This study was financially supported by The Iwatani Naoji Foundation.

Appendix A. Supplementary data

Supplementary data to this article can be found online at https://doi.org/XXXXX. Video of the deposition/dissolution process (video).

References

[1] M. Winter, J.O. Besenhard, M.E. Spahr, P. Novák, Adv. Mater., 10 (1998) 725-763.

[2] L. Li, S. Li, Y. Lu, Chem. Commun., 54 (2018) 6648-6661.

[3] M. Yamagata, Y. Matsui, T. Sugimoto, M. Kikuta, T. Higashizaki, M. Kono, M. Ishikawa, J. Power Sources, 227 (2013) 60-64.

[4] X.-B. Cheng, R. Zhang, C.-Z. Zhao, Q. Zhang, Chem. Rev., 117 (2017) 10403-10473.

[5] W. Xu, J. Wang, F. Ding, X. Chen, E. Nasybulin, Y. Zhang, J.-G. Zhang, Energy Environ. Sci., 7 (2014) 513-537.

[6] X.-B. Cheng, R. Zhang, C.-Z. Zhao, F. Wei, J.-G. Zhang, Q. Zhang, Adv. Sci., 3 (2016) 1500213.

[7] B. Scrosati, J. Hassoun, Y.-K. Sun, Energy Environ. Sci., 4 (2011) 3287-3295.

[8] S. Xin, L. Gu, N.-H. Zhao, Y.-X. Yin, L.-J. Zhou, Y.-G. Guo, L.-J. Wan, J. Am. Chem. Soc., 134 (2012) 18510-18513.

[9] Z. Ma, X. Yuan, L. Li, Z.-F. Ma, D.P. Wilkinson, L. Zhang, J. Zhang, Energy Environ. Sci., 8 (2015) 2144-2198.

[10] D. Lin, Y. Liu, Y. Cui, Nat. Nanotechnol., 12 (2017) 194.

[11] F. Ding, W. Xu, X. Chen, J. Zhang, M.H. Engelhard, Y. Zhang, B.R. Johnson, J.V. Crum, T.A. Blake, X. Liu, J.-G. Zhang, J. Electrochem. Soc., 160 (2013) A1894-A1901.

[12] L. Li, S. Zhou, H. Han, H. Li, J. Nie, M. Armand, Z. Zhou, X. Huang, J. Electrochem. Soc., 158 (2011) A74-A82.

[13] Y. Matsuda, M. Sekiya, J. Power Sources, 81-82 (1999) 759-761.

[14] H. Yue, Y. Yang, Y. Xiao, Z. Dong, S. Cheng, Y. Yin, C. Ling, W. Yang, Y. Yu, S. Yang, J. Mater. Chem. A, 7 (2019) 594-602.

[15] A.M. Tripathi, W.-N. Su, B.J. Hwang, Chem. Soc. Rev., 47 (2018) 736-851.

[16] S. Li, M. Jiang, Y. Xie, H. Xu, J. Jia, J. Li, Adv. Mater., 30 (2018) 1706375.

[17] B. Tong, J. Huang, Z. Zhou, Z. Peng, Adv. Mater., 30 (2018) 1704841.

[18] Q.-C. Liu, J.-J. Xu, S. Yuan, Z.-W. Chang, D. Xu, Y.-B. Yin, L. Li, H.-X. Zhong, Y.-S. Jiang, J.-M. Yan, X.-B. Zhang, Adv. Mater., 27 (2015) 5241-5247.

[19] H. Lee, D.J. Lee, Y.-J. Kim, J.-K. Park, H.-T. Kim, J. Power Sources, 284 (2015) 103-108.

[20] Y. Liu, D. Lin, P.Y. Yuen, K. Liu, J. Xie, R.H. Dauskardt, Y. Cui, Adv. Mater., 29 (2017) 1605531.

[21] J. Alvarado, M.A. Schroeder, T.P. Pollard, X. Wang, J.Z. Lee, M. Zhang, T. Wynn, M. Ding, O. Borodin, Y.S. Meng, K. Xu, Energy Environ. Sci., 12 (2019) 780-794.

[22] C. Wan, S. Xu, M.Y. Hu, R. Cao, J. Qian, Z. Qin, J. Liu, K.T. Mueller, J.-G. Zhang, J.Z. Hu, ACS Appl. Mater. Interfaces, 9 (2017) 14741-14748.

[23] R. Miao, J. Yang, Z. Xu, J. Wang, Y. Nuli, L. Sun, Sci. Rep., 6 (2016) 21771.

[24] J. Qian, W.A. Henderson, W. Xu, P. Bhattacharya, M. Engelhard, O. Borodin, J.-G. Zhang, Nat. Commun., 6 (2015) 6362.

[25] C. Sun, T. Wu, J. Wang, W. Li, J. Jin, J. Yang, Z. Wen, J. Mater. Chem. A, 6 (2018) 19159-19166.

[26] H. Kim, F. Wu, J.T. Lee, N. Nitta, H.-T. Lin, M. Oschatz, W.I. Cho, S. Kaskel, O. Borodin, G. Yushin, Adv. Energy. Mater., 5 (2015) 1401792.

[27] S. Xiong, Y. Diao, X. Hong, Y. Chen, K. Xie, J. Electroanal. Chem., 719 (2014) 122-126.

[28] H. Yoon, G.H. Lane, Y. Shekibi, P.C. Howlett, M. Forsyth, A.S. Best, D.R. MacFarlane, Energy Environ. Sci., 6 (2013) 979-986.

[29] D. Aurbach, E. Zinigrad, Y. Cohen, H. Teller, Solid State Ionics, 148 (2002) 405-416.

[30] S. Hess, M. Wohlfahrt-Mehrens, M. Wachtler, J. Electrochem. Soc., 162 (2015) A3084-A3097.

[31] A. Basile, A.I. Bhatt, A.P. O'Mullane, Nat. Commun., 7 (2016) 11794.

[32] N. Schweikert, A. Hofmann, M. Schulz, M. Scheuermann, S.T. Boles, T. Hanemann, H. Hahn, S. Indris, J. Power Sources, 228 (2013) 237-243.

[33] H. Sano, M. Kitta, H. Matsumoto, J. Electrochem. Soc., 163 (2016) D3076-D3079.

[34] F. Mizuno, T.S. Arthur, K. Takechi, ACS Energy Letters, 1 (2016) 542-547.

[35] N.-W. Li, Y.-X. Yin, J.-Y. Li, C.-H. Zhang, Y.-G. Guo, Adv. Sci., 4 (2017) 1600400.

[36] J.M. Clark, S.-i. Nishimura, A. Yamada, M.S. Islam, Angew. Chem. Int. Ed., 51 (2012) 13149-13153.

[37] H. Sano, H. Sakaebe, H. Matsumoto, J. Power Sources, 196 (2011) 6663-6669.

[38] K.-H. Chen, K.N. Wood, E. Kazyak, W.S. LePage, A.L. Davis, A.J. Sanchez, N.P. Dasgupta, J. Mater. Chem. A, 5 (2017) 11671-11681.

[39] A. Basile, A.F. Hollenkamp, A.I. Bhatt, A.P. O'Mullane, Electrochem. Commun., 27 (2013) 69-72.

[40] G. Bieker, M. Winter, P. Bieker, Phys. Chem. Chem. Phys., 17 (2015) 8670-8679.

[41] J. Hwang, K. Matsumoto, R. Hagiwara, J. Phys. Chem. C, 122 (2018) 26857-26864.

[42] N. Ogihara, Y. Itou, T. Sasaki, Y. Takeuchi, J. Phys. Chem. C, 119 (2015) 4612-4619.

[43] L. Fan, S. Li, L. Liu, W. Zhang, L. Gao, Y. Fu, F. Chen, J. Li, H.L. Zhuang, Y. Lu, Adv. Energy Mater., 8 (2018) 1802350.

[44] P.H. Citrin, G.K. Wertheim, Y. Baer, Phys. Rev. B, 16 (1977) 4256-4282.

[45] L. Suo, Y.-S. Hu, H. Li, M. Armand, L. Chen, Nat. Commun., 4 (2013) 1481.

[46] S.E. Sloop, J.K. Pugh, S. Wang, J.B. Kerr, K. Kinoshita, Electrochem. Solid-State Lett., 4 (2001) A42-A44.

[47] M. Wang, L. Huai, G. Hu, S. Yang, F. Ren, S. Wang, Z. Zhang, Z. Chen, Z. Peng, C. Shen, D. Wang, J. Phys. Chem. C, 122 (2018) 9825-9834.